Can oxygen utilization rate be used to track the long-term changes of aerobic respiration in the mesopelagic Atlantic Ocean?

Haichao Guo[1], Iris Kriest[1], Andreas Oschlies[1], and Wolfgang Koeve[1]

[1]GEOMAR Helmholtz Centre for Ocean Research Kiel, 24105, Kiel, Germany

Key Points:

- Our model study confirms earlier findings that oxygen utilization rate (OUR) underestimates true respiration (R_{true}) in mesopelagic ocean
- Despite OUR underestimate R_{true}, OUR can adequately estimate long-term changes in R_{true} in the mesopelagic North Atlantic subtropical gyre
- OUR cannot adequately estimate climate-driven changes in R_{true} in the mesopelagic tropical South Atlantic where different water masses mix.

Corresponding author: Haichao Guo, `hguo@geomar.de`

Abstract

Quantifying changes in oceanic aerobic respiration is essential for understanding marine deoxygenation. Here we use an Earth system model to investigate if and to what extent oxygen utilization rate (OUR) can be used to track the temporal change of true respiration (R_{true}). R_{true} results from the degradation of particulate and dissolved organic matter in the model ocean, acting as ground truth to evaluate the accuracy of OUR. Results show that in thermocline and intermediate waters of the North Atlantic Subtropical Gyre (200m-1000m), vertically integrated OUR and R_{true} both decrease by 0.2 $\text{molO}_2/\text{m}^2/\text{yr}$ from 1850 to 2100 under global warming. However, in the mesopelagic Tropical South Atlantic, integrated OUR increases by 0.2 $\text{molO}_2/\text{m}^2/\text{yr}$, while the R_{true} integral decreases by 0.3 $\text{molO}_2/\text{m}^2/\text{yr}$. A possible reason for the diverging OUR and R_{true} is ocean mixing, which affects water mass composition and maps remote respiration changes to the study region.

Plain Language Summary

The ocean is losing oxygen due to an imbalance in oxygen supply and aerobic respiration. Therefore, monitoring temporal changes in the aerobic respiration rate contributes to understanding marine deoxygenation. Based on simulations of an Earth system model, we investigate an indirect diagnostic measure of the respiration rate (oxygen utilization rate, OUR), calculated as the slope of the least square regression of the apparent oxygen utilization (AOU, saturated oxygen concentration minus local oxygen concentration) and seawater age that can be computed from transient abiotic tracers. As the reference to OUR, true respiration (R_{true}) is the oxygen consumption rate resulting from the degradation of organic matter in the model ocean. Results show that in the North Atlantic Subtropical Gyre intermediate water (200m-1000m), both vertically integrated OUR and R_{true} decrease by 0.2 $\text{molO}_2/\text{m}^2/\text{yr}$ from 1850 to 2100. However, in the Tropical South Atlantic intermediate water, the OUR integral increases by 0.2 $\text{molO}_2/\text{m}^2/\text{yr}$ and the R_{true} integral decreases by 0.3 $\text{molO}_2/\text{m}^2/\text{yr}$. We hypothesize that changes in ocean mixing over time, which can affect water mass composition and map remote respiration changes to the study region, explain the discrepancy of OUR and R_{true} tendencies.

1 Introduction

Observations suggest that the dissolved oxygen concentration in the ocean has been substantially declining over the past 50 yrs (Schmidtko et al., 2017; Ito et al., 2017). This deoxygenation process has far-reaching impacts on global ocean ecosystems and biogeochemical processes (Stramma et al., 2008; Breitburg et al., 2018; Pezner et al., 2023). Better understanding ocean deoxygenation requires quantitatively assessing the temporal changes in the oxygen supply and sink processes, i.e., (i) oxygen solubility at the surface, (ii) ventilation, and (iii) aerobic respiration (Oschlies et al., 2018; Robinson, 2019).

While the contribution of (i) can straightforwardly be estimated from observations and was found to explain about 15% of the observed decline in oceanic oxygen inventory from 1960 to 2010 (Schmidtko et al., 2017), contributions from (ii) and (iii) are more difficult to quantify. Here we address (iii), i.e. changes in aerobic respiration.

Direct measurements of respiration rates over the recent decades are still sparse because of methodological limitations (Del Giorgio & Williams, 2005; Robinson, 2019). For example, rates obtained via enzymatic ETS (electron transport system) represent potential rates and are thus only a proxy for microbial activity, which has to be converted to actual respiration rates. This conversion is not always straightforward as it depends on community composition of organisms (Filella et al., 2018), which might change quickly in space and time. Likewise, rates obtained through oxygen uptake in sea water incu-

bations integrate over the entire auto- and heterotrophic community, and depend on the availability of organic substrate. They may thus also represent just a snapshot of biogeochemical processes at a certain location. On the other hand, respiration estimates calculated from the decay of particle flux with depth, integrate over larger space and longer time scales, but are affected by mixing and advection that may laterally decouple the signals recorded at different depths (Waniek et al., 2000). In this case, it can be difficult to disentangle the effects of the hydrodynamic components from the biological ones.

Here, we focus on the classic Oxygen Utilization Rate (OUR) method as an indirect measure of marine respiration. OUR is defined as the slope of the least square regression of apparent oxygen utilization (AOU, the difference between saturated oxygen concentration, $[O_2^{\text{sat}}]$, and actual oxygen concentration, $[O_2^{\text{obs}}]$) and seawater age (t) on potential density surfaces (equation 1; Jenkins, 1987). Seawater age is defined as the time elapsed since the water had been last in contact with the atmosphere. Notably, AOU might overestimate the true oxygen utilization (TOU) due to an incomplete equilibration of the sea surface oxygen (Ito et al., 2004; Duteil et al., 2013). Still, instead of using AOU directly as proxy for respiration, OUR is determined by the regression between AOU and the seawater age. The OUR derived from AOU would not differ much from that derived from TOU if water parcels share the same biases from surface disequilibration and thus do not affect isopycnal oxygen utilization gradients (Sonnerup et al., 2019).

In the real ocean, AOU is a readily available property of seawater, while the age of a water mass is typically derived from transient abiotic tracers like sulphur hexafluoride (SF6), chlorofluorocarbons (CFCs, e.g. CFC-11, CFC-12), or radioactive elements (e.g. ^{3}H, ^{39}Ar, ^{14}C) (Fine, 2011; Fine et al., 2017; Stöven et al., 2015). These age tracers have been intensively measured globally over the last three decades (Fine et al., 2017), which allows, theoretically, the widespread use of OUR and reconstruction of respiration over decades in parts of the ocean. Note that current approaches to estimate seawater age (e.g., tracer age, transient time distribution TTD) still include some uncertainties and biases, like the assumption of perfect saturation of transient tracers at the time of water mass formation (Stöven et al., 2015).

$$OUR = \frac{\partial AOU}{\partial t} = \frac{\partial([O_2^{\text{sat}}] - [O_2^{\text{obs}}])}{\partial t} \tag{1}$$

Despite several field studies (e.g., Jenkins, 1987; Brea et al., 2004; Sonnerup et al., 2013, 2015, 2019; Álvarez-Salgado et al., 2014) and model studies (e.g., Koeve & Kähler, 2016) focusing on the comparison between OUR and other independent respiration estimations at specific time points, to our knowledge, no study has attempted to evaluate the potential ability of OUR on tracking temporal changes in aerobic respiration under a changing climate. One reason might be the above-mentioned difficulties in obtaining direct observations of in-situ respiration rates in the real ocean as OUR reference. Here, we employ a high-resolution Earth system model (for which we have perfect spatial and temporal coverage of "sampling", and knowledge of the true respiration rate) to address this issue. In particular, we examine the relationship and its temporal variations between OUR (calculated from simulated AOU and ideal age) and true respiration from 1850 to 2100 for a global warming scenario in two selected study areas in the Atlantic Ocean.

2 Method

2.1 Model description

The model used in this study is the Flexible Ocean and Climate Infrastructure (FOCI) Earth system model (Matthes et al., 2020) coupled to ocean biogeochemistry as detailed by Chien et al. (2022). It includes an atmosphere, a land biosphere, an ocean circula-

tion, a sea-ice, and an ocean biogeochemistry component. The oceanic components apply the ORCA05 grid, corresponding to a tripolar grid with $0.5° \times 0.5°$ nominal horizontal resolution and 46 vertical levels with thicknesses varying from 6 m at the surface to 250 m in the deep ocean. Tracer diffusion is aligned along isopycnals, with a diffusion coefficient of $600 \text{ m}^2\text{s}^{-1}$. The biogeochemical component of FOCI, MOPS (Model of Oceanic Pelagic Stoichiometry) includes nine compartments, of which five are calculated in phosphorus units, namely phytoplankton, zooplankton, particulate detritus (DET), dissolved organic matter (DOM), and phosphate. The abiotic tracers include oxygen, nitrate, dissolved inorganic carbon, and alkalinity (Kriest & Oschlies, 2015; Chien et al., 2022). The effects of iron limitation on marine primary productivity are not explicitly resolved in MOPS. With some modifications due to a slow-down of respiration in low-oxygen environments (see Kriest & Oschlies, 2015; Chien et al., 2022), the flux profile of particulate organic matter in MOPS follows a "Martin Curve" (Martin et al., 1987), where the exponent is derived from a constant decay rate (0.05 d^{-1}) and linearly increasing sinking speed $(w = 0.0354\,z \text{ m/d})$.

We here describe details on how FOCI simulates ideal age and true respiration rate. The ideal age tracer works like a "clock," which increases one day per day since the water parcel has left the surface. The "clock" is set to zero when the water reaches the surface of the ocean (Thiele & Sarmiento, 1990). In FOCI, the ideal age is set to zero in the upper 10 m. The remineralization rate in MOPS is temperature-independent and depends only on substrate availability and oxygen concentration. Oxygen concentration constrains remineralization rate only in the oxygen deficit zone, which is not the case for the two sections analyzed here. Hence, we do not need to account for the oxygen dependence of remineralization in this paper, but refer readers to Chien et al. (2022, Appendix A1) for details. The true respiration rate, R_{true}, is the oxygen consumption rate for aerobic remineralization of DET and DOM in each grid box, as described in Equation 2:

$$R_{\text{true}} = (\lambda'_{\text{DET}} \cdot DET + \lambda'_{\text{DOM}} \cdot DOM) \cdot R_{\text{O2:P}} \qquad (2)$$

where λ'_{DET} (0.05d^{-1}) and λ'_{DOM} (0.17yr^{-1}) are the temperature-independent decay rates of DET and DOM, respectively. $R_{\text{O2:P}} = 165.08044$ denotes the calibrated stoichiometric oxygen demand of aerobic remineralization (Chien et al., 2022). R_{true} is computed at every model time step and acts as the ground truth of its proxy, OUR, in the model ocean.

The experimental set-up is detailed by Chien et al. (2022), and we show the schematic figure (Figure S1) and some technical details in the supplementary material Text S1. In brief, the model was integrated for 750 years under a pre-industrial partial pressure of CO_2 as a total spin-up. Branching off from this spinup state, transient climate-change and pre-industrial control (esm-piControl) simulations were carried out for 250 years, respectively. The transient simulations include 165 years (1850 to 2014) historical simulation and 85 years (2015 to 2099) projection under the Shared Socioeconomic Pathways 585 (SSP-585) scenario (esm-ssp-585; Eyring et al., 2016). The esm-piControl simulation shares the same time period as transient simulations but without anthropogenic effects (zero-emission of CO_2). Concerning the model's projection sensitivity to initial conditions and spin-up, three transient simulations and esm-piControl simulations were employed. These simulations branch off from the 730th, 740th, and 750th year of the spin-up simulation, respectively (for brevity simply referred to as ensemble members 1, 2, 3). Here, we only present details of ensemble member 1, but provide the statistical analysis of simulated OUR and true respiration for all ensemble members in Table 1 to support the robustness of the finding.

2.2 Model analysis

We confine our analysis to the mesopelagic zone, i.e. the depth range 200m to 1000m. We consider OUR estimates unreliable in the upper 200m because of possible seasonal effects such as subsurface warming by absorption of solar radiation (e.g., Dietze & Oschlies, 2005). In addition, AOU is also substantially modified by photosynthesis in the photic zone. In the deep ocean below 1000m, respiration proceeds at a very low rate (Del Giorgio & Duarte, 2002; Williams, 1981). Although 76% of total ocean volume is below 1000m, the respiration in the ocean interior only contributes 3% of globally integrated oceanic respiration in the FOCI model.

We select two main study sections, referred to as the North Atlantic Subtropical Gyre (NASG section, 60°W-30°W, 20°N-25°N) and the Tropical South Atlantic (TSA section, 35°W-5°W, 15°S-20°S), respectively (Figure 1). Both sections approximately fit the criteria for selecting sections used by Jenkins (1987): (a) sections should follow the advective flow direction (Figure S2) and (b) should be approximately perpendicular to isolines of ideal age and AOU. These conditions are considered necessary criteria to minimize the effects of mixing of different source water types, which could otherwise misguide attempts to estimate local respiration rates from OUR. Also, the NASG region was selected since it is one of the regions projected to suffer the most significant reduction of net primary production in climate projections, though with large uncertainties (Kwiatkowski et al., 2020; Tagliabue et al., 2021). This might impact local respiration rates and oxygen concentrations. Finally, the NASG and TSA sections experience different circulation patterns and water masses compositions (Poole & Tomczak, 1999), which might lead to a different behaviour of OUR under a changing climate.

Along the chosen sections, we compare the diagnosed OUR and the true respiration, integrated vertically over the mesopelagic zone rather than on individual density surfaces. We notice a sharp change of density surface depth in the transient simulations, e.g., in the NASG section, the depth of potential density surface 26.5 kg/m^3 increases from 257.1 ± 51.4 to 420.7 ± 4.3 m from 1850 to 2099. Such changes of isopycnal mean depth can, in itself, induce significant changes in the true respiration on the respective density surfaces (Figure S3). Vertical displacement of isopycnals may mislead the analysis of how the biology-induced respiration evolves under changing climate. Hence we decide to explore temporal trends of vertically integrated R_{true} and OUR in this study.

We derive the vertical integrals of R_{true} and OUR from 200m to 1000m as follows. Firstly, we calculate the potential density from potential temperature, salinity, and surface reference pressure (0 decibar) using the 1980 UNESCO International Equation of State (Millero & Poisson, 1981), and remap data from z-coordinates to sigma0-coordinates. The OUR is calculated for every 0.1 kg/m^3 density surface interval from 24.1 to 28.0 kg/m³ by using the linear least square regression of AOU versus ideal age. We also calculate the area-weighted mean true respiration and mean depth for each density surface. Afterwards, we remap OUR and mean R_{true} onto z-coordinates using the area-weighted depth of the corresponding density surfaces. Finally, the vertical integral is obtained as the sum of the density layer thickness times the variable (OUR or mean R_{true}) at each grid point; see details in the supplementary material Text S2. The transformation of coordinates forth and back does not induce biases on either the vertical distribution of true respiration rate or the trend of integrated R_{true} (Figure S4).

3 Results and discussion

Depth (200m to 1000m) integrated OUR underestimates integrated R_{true} along the NASG section by around 1.9 fold (Figure 2a), and most of the underestimation occurs in the upper ocean (Figure 2b). This underestimate may be caused by the spatial heterogeneity of respiration on isopycnals, as found for idealized isopycnals with prescribed
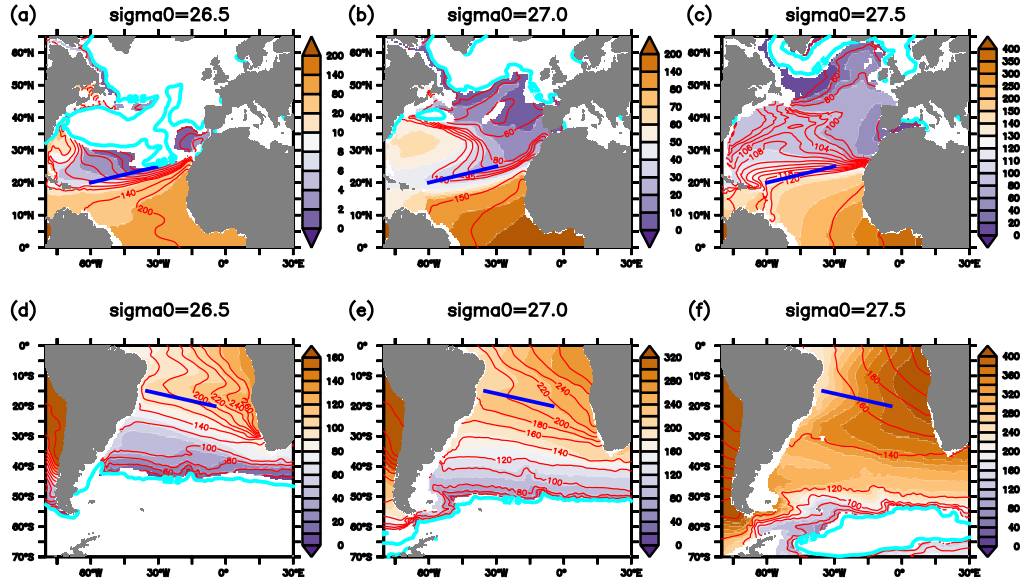
Figure 1. Distributions of ideal age (shading), AOU (red lines), and outcrop locations (light-blue lines) in the North and the South Atlantic Ocean on three isopycnal surfaces. We use the 2090-2099 mean in the esm-piControl simulation and exclude the waters above the respective hemispheric winter mixing depth. Winter surface density outcrops are calculated from March (northern hemisphere) and September (southern hemisphere) mean temperature and salinity. Blue lines represent chosen study sections.

patterns of respiration (Koeve & Kähler, 2016). High respiration occurs near the outcrops (shallower ocean) due to the high availability of substrates and low sinking speed of detritus. But, mixing with nearby surface waters (with high oxygen concentration) does not allow the imprint of respiration, AOU, to be well preserved. On the other hand, respiration far from outcrops (deeper ocean) can be better preserved in terms of AOU because of smaller mixing losses to surface waters. However, respiration in deeper waters is often much lower because much organic matter has already been consumed in the water column above, and because the sinking speed of particulate organic matter increases with depth (Berelson, 2001). In contrast to respiration, the water aging rate is the same everywhere. Therefore, more of the idealized age tracer is preserved on isopycnals compared to AOU, and consequently the OUR diagnosed from the ratio of AOU gradient to ideal age gradient is smaller than R_{true}. The underestimate of OUR compared to the R_{true}, and the vertical distribution of their difference, has also been found in the other two ensemble members with similar magnitude (Table 1, Figure S5ab, S6ab).

At the 95% confidence level, the esm-piControl experiment shows an OUR trend of -0.241 ±0.239 mmol/m^2/yr^2, while the trend of true respiration is +0.282±0.191 mmol/m^2/yr^2 along the NASG section (Figure 2c). These small drifts in the true respiration and OUR in the esm-piControl simulations might result from a too short spin-up or from internal variability in the Earth system model (Matthes et al., 2020). Over the entire period from 1850 to 2100, the Pearson correlation coefficient between the diagnosed OUR and the true respiration in esm-piControl is 0.48.

The true respiration along the NASG section shows a long-term drift-corrected decreasing trend along with global warming in the transient simulations (Figure 2d). Here we use the transient simulation minus esm-piControl to remove the trend in the latter and isolate the climate change signal. The true respiration decreases with the rate of 0.872 ± 0.268 mmol/m^2/yr^2 from 1850 to 2100, indicating a total decline of up to 10.6 % of local mesopelagic respiration. Overall, mesopelagic respiration is reduced by about 0.2 mmol/m^2/yr in the NASG section by the end of this century. Average trend and total decline are the same in the other two ensemble members at the 95% confidence level (Table 1). A decline in respiration can be related to enhanced stratification (Figure S9a) and reduced nutrient supply, as has been suggested as an explanation for reduced net primary production in the tropical and temperate regions in earlier model simulations (Bopp et al., 2013; Kwiatkowski et al., 2020).

For the high emission climate change scenario simulated here, the drift-corrected vertical OUR integral is suitable to track the long-term trend of the vertical R_{true} integral along the NASG section (Figure 2d). The OUR integral trend is -0.802 ± 0.333 mmol/m^2/yr^2, which overlaps statistically with the R_{true} changes of -0.872 ± 0.268 mmol/m^2/yr^2. Besides, the Pearson correlation coefficient between the diagnosed OUR integral and R_{true} integral is 0.54 for the transient minus esm-piControl. In the other two ensemble members, the trends of OUR and R_{true} integral versus time also overlap at the 95% confidence level (Table 1).

In our second study region, the TSA section, the vertically integrated OUR amounts to 83.3% of the R_{true} integral in the esm-piControl simulation (Figure 3a), and the underestimation of true respiration by OUR occurs between 200m and 300m (Figure 3b). A similar explanation as put forward for the NASG section above can be proposed here. Below around 320m, however, OUR overestimates true respiration and even increases with depth between 300m to 400m (Figure 3b). Both vertical integrals of OUR and R_{true} do not show a significant temporal trend in the esm-piControl simulation of the ensemble member 1 (Figure 3c), but the Pearson correlation coefficient between them is only 0.193. When calculating the transient tendencies corrected by the esm-piControl, vertically integrated OUR and R_{true} show significantly diverging trends (Figure 3d). The R_{true} integral decreases with a rate of 1.311±0.197 mmol/m^2/yr^2, i.e., between 1850 and 2100, mesopelagic respiration decreases by about 0.3 mmol/m^2/yr. In contrast, the OUR
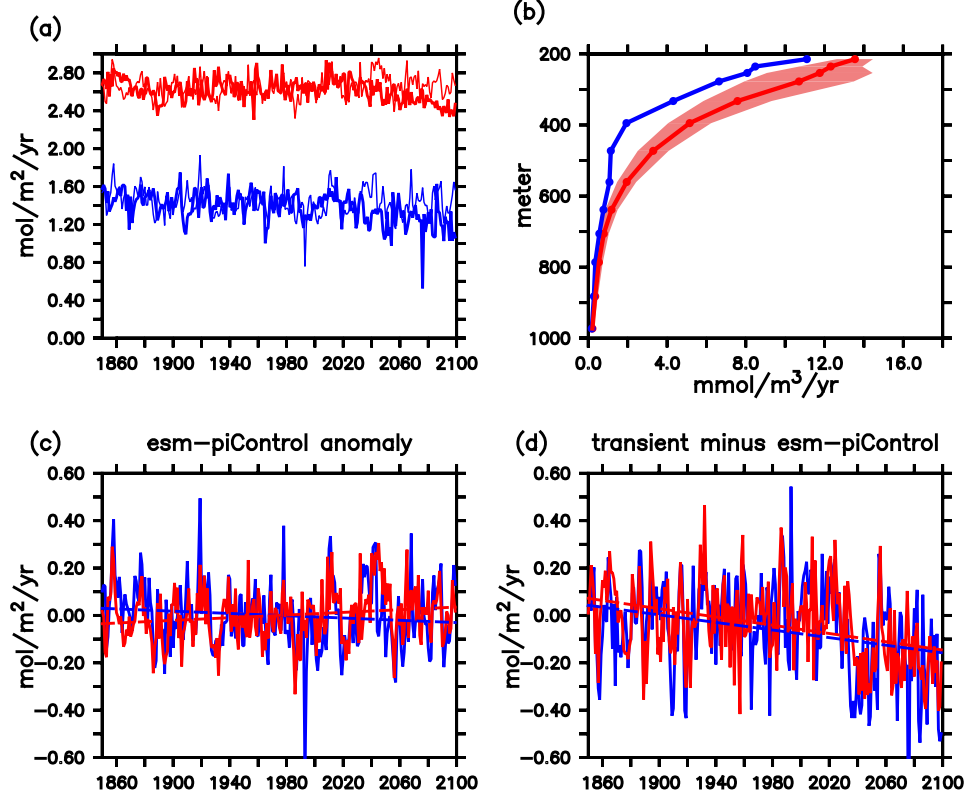
Figure 2. Comparison between vertically integrated OUR and true respiration (200 - 1000m) along the NASG section (see blue line in Figure 1a) in simulation ensemble member 1. Panel (a) shows absolute vertically integrated OUR (blue) and true respiration (red) from the transient simulation (thick) and the esm-piControl simulation (thin). Panel (b) is the vertical distribution of OUR (blue) and true respiration (red) in the last year of the esm-piControl simulation. The shading indicates one standard deviation, while OUR standard deviation is too small to be visible. All r^2 values of the linear regressions of AOU against ideal age on density surfaces are above 0.92. Panel (c) shows the integrated OUR (thick blue line) and true respiration (thick red line) anomalies relative to the respective time-averaged values of the esm-piControl simulation. The thin solid lines are the linear least square regression lines of integrated OUR anomalies (blue) and integrated true respiration anomalies (red) over time. (d) shows the transient minus esm-piControl integrated OUR (blue) and true respiration (red), and their linear least square regression lines over time.
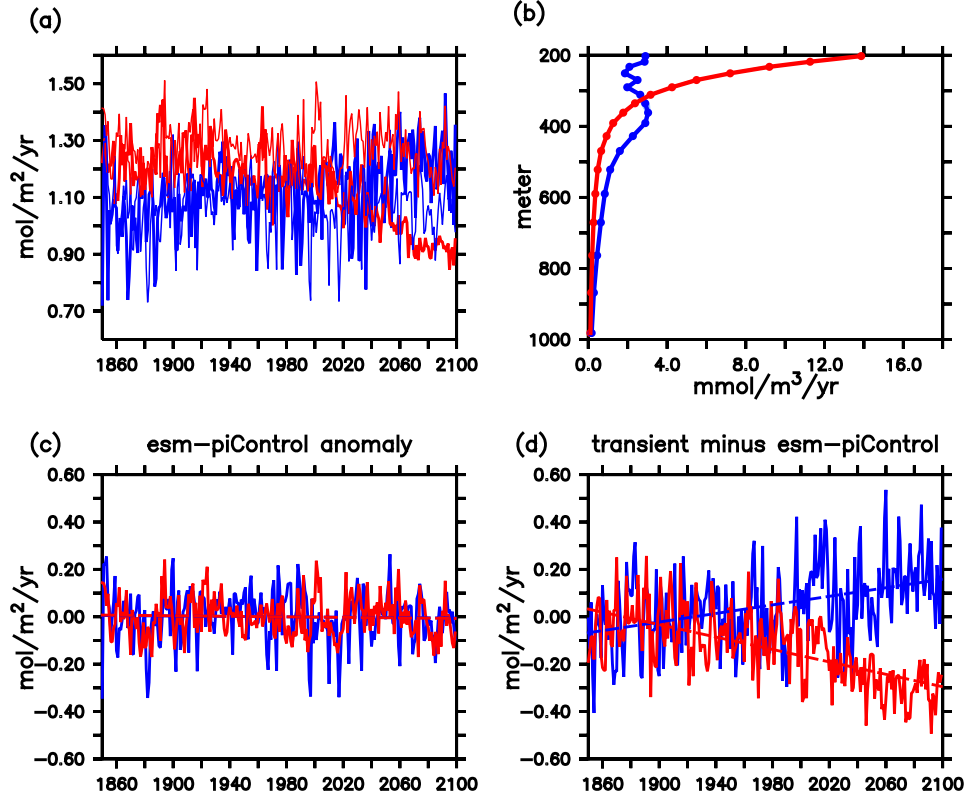
Figure 3. As Figure 2, but for the TSA section (see blue line in Figure 1d). In panel (b), all r^2 values of the linear regressions of AOU against ideal age on density surfaces are above 0.94. The standard deviation of true respiration rates and OUR is too small to be visible.

integral shows a significant increasing trend of 0.905 ± 0.257 mmol/m^2/yr^2. In other words, OUR integral suggests that the mesopelagic respiration in the TSA section will increase by 0.2 mmol/m^2/yr by 2100. The other two ensemble members show similar features (Table 1, Figure S7, S8). To sum up the above results, we propose that along the TSA section, the trend of the OUR integral is not primarily determined by changes in local respiration.

What are potential reasons for the diverging trends in the vertical integrals of OUR and local true respiration (R_{true}) along the TSA section? First, local R_{true} decreases with time, likely because of the enhanced stratification (Figure S9a) as seen also at the NASG section and in other model results (Bopp et al., 2013; Kwiatkowski et al., 2020). The increasing OUR may indicate either an increasing AOU gradient along the section, decreasing age gradient, or a combination of both (see Equation 1). Here we propose two possible reasons for the increasing OUR in the TSA section: (i) Ocean circulation changes in a warming ocean might change water mass composition in the study region, that is water masses with different biogeochemical histories are recombined over time in different ways, potentially causing a change in tracer distribution, e.g. a steepening of the AOU versus age regression line. (ii) In regions where source water masses observed in the study region form, ocean biogeochemistry also responds to climate change. For example, in the region of formation of Subantarctic Mode Waters (SAMW), we found a strong increase

Table 1. Ratio of vertically (200m to 1000m) integrated true respiration (R_{true}) and OUR, trend of R_{true} and OUR over time and its 95% confidence interval, and Pearson correlation coefficient between integrated R_{true} and OUR (with p-value below 0.05). "n.s." represents the non-significant outcomes (with p-value above 0.05).

Region	simulations	ensemble members	R_{true}/OUR	trend of R_{true}[a] (mmol/m^2/yr^2)	trend of OUR[a] (mmol/m^2/yr^2)	correlation coefficient
NASG	esm-piControl	1	1.9	0.282±0.191	-0.241 ±0.239	0.48
		2	1.9	n.s.	-0.288±0.246	0.51
		3	1.9	0.433±0.205	n.s.	0.45
	transient minus esm-piControl	1	1.9	-0.872±0.268	-0.802±0.333	0.54
		2	1.9	-0.833±0.296	-0.844±0.357	0.54
		3	1.9	-0.981±0.272	-0.754±0.362	0.55
TSA	esm-piControl	1	1.2	n.s.	n.s.	0.19
		2	1.2	0.206±0.137	n.s.	0.13
		3	1.2	0.191±0.150	-0.316±0.188	n.s.
	transient minus esm-piControl	1	1.0	-1.311±0.197	0.905±0.257	-0.19
		2	1.0	-1.783±0.200	0.520±0.268	n.s.
		3	1.0	-1.323±0.182	0.826±0.257	-0.17

[a] For trends: positive number means increase and negative number means decrease.

in true respiration (Figure S9b). The associated AOU can then propagate with the SAMW into the study region and impact the regression relationship between AOU and age. All the above processes may be summed as an 'apparent' OUR contribution induced by the mixing-driven intrusion of AOU and age signals from outside of the study section. For clarification, we suggest to rewrite the OUR equation as follows:

$$OUR = R_{\text{true}} + OUR_{\text{mixing}} \tag{3}$$

in which, R_{true} is local OUR induced by the degradation of DOM and DET along the section, and OUR_{mixing} is 'apparent' OUR induced by the mixing of waters from different origins, yielding imprints of ocean biogeochemistry and water age from outside the study section (Sonnerup et al., 1999). We hypothesize that depending on the region under consideration, R_{true} might be either the main (e.g., in the NASG section) or a minor driver (e.g., in the TSA section) of OUR change.

To reliably infer temporal changes in R_{true} from OUR under global warming, it is required to remove the mixing-induced contributions to AOU and age. This has been addressed in several studies assuming steady-state conditions, e.g. by applying the Optimal Multi-Parameter (OMP) analysis (e.g., Karstensen & Tomczak, 1998; Brea et al., 2004; Álvarez-Salgado et al., 2014). However, this method requires temporally constant properties (e.g., potential temperature, salinity) of water masses in their formation regions (Álvarez et al., 2014), which may limit its straightforward application in a changing ocean.

4 Conclusions

Our study confirms the potential ability of OUR to track the trends of true respiration during the time period between 1850 and 2100, and may hence contribute to our understanding of drivers of ocean deoxygenation in parts of the ocean. However, there is also a risk that temporal trends diagnosed from OUR can be an unreliable indicator of trends in true respiration, and may even be of opposite sign to trends of true respiration in other parts of the ocean (as in the example of the tropical South Atlantic). As one potential reason of diverging trends between local respiration and OUR, we propose

that climate-driven changes in ocean mixing, in water mass composition and in biogeo-
chemical properties of individual water masses can map onto the local OUR. A quan-
tification of climate-driven changes in aerobic respiration from OUR requires separat-
ing mixing-induced changes in AOU and age, including temporal changes of water masses
composition and properties. This is challenging, as it requires careful consideration of
climate-driven changes in (remote) areas of water mass formation, whenever mixing of
multiple water masses is involved.

5 Data availability statement

The model code is provided by Chien et al. (2022) at https://doi.org/10.5281/zenodo.6772175.
The model outputs used in this paper, together with the scripts for data processing are
available at: https://hdl.handle.net/20.500.12085/e7d53204-df0c-4973-8628-63dad7dd140.

References

Álvarez, M., Brea, S., Mercier, H., & Álvarez-Salgado, X. A. (2014). Mineralization of biogenic materials in the water masses of the south atlantic ocean. i: Assessment and results of an optimum multiparameter analysis. *Progress in Oceanography*, *123*, 1–23.

Álvarez-Salgado, X. A., Álvarez, M., Brea, S., Mémery, L., & Messias, M. (2014). Mineralization of biogenic materials in the water masses of the south atlantic ocean. ii: Stoichiometric ratios and mineralization rates. *Progress in Oceanography*, *123*, 24–37.

Berelson, W. M. (2001). Particle settling rates increase with depth in the ocean. *Deep Sea Research Part II: Topical Studies in Oceanography*, *49*(1-3), 237–251.

Bopp, L., Resplandy, L., Orr, J. C., Doney, S. C., Dunne, J. P., Gehlen, M., ... others (2013). Multiple stressors of ocean ecosystems in the 21st century: projections with cmip5 models. *Biogeosciences*, *10*(10), 6225–6245.

Brea, S., Álvarez-Salgado, X. A., Álvarez, M., Pérez, F. F., Mémery, L., Mercier, H., & Messias, M.-J. (2004). Nutrient mineralization rates and ratios in the eastern south atlantic. *Journal of Geophysical Research: Oceans*, *109*(C5).

Breitburg, D., Levin, L. A., Oschlies, A., Grégoire, M., Chavez, F. P., Conley, D. J., ... others (2018). Declining oxygen in the global ocean and coastal waters. *Science*, *359*(6371), eaam7240.

Chien, C.-T., Durgadoo, J. V., Ehlert, D., Frenger, I., Keller, D. P., Koeve, W., ... others (2022). Foci-mops v1–integration of marine biogeochemistry within the flexible ocean and climate infrastructure version 1 (foci 1) earth system model. *Geoscientific Model Development*, *15*(15), 5987–6024.

Del Giorgio, P., & Duarte, C. M. (2002). Respiration in the open ocean. *Nature*, *420*(6914), 379–384.

Del Giorgio, P., & Williams, P. (2005). *Respiration in aquatic ecosystems*. OUP Oxford.

Dietze, H., & Oschlies, A. (2005). Modeling abiotic production of apparent oxygen utilisation in the oligotrophic subtropical north atlantic. *Ocean Dynamics*, *55*, 28–33.

Duteil, O., Koeve, W., Oschlies, A., Bianchi, D., Galbraith, E., Kriest, I., & Matear, R. (2013). A novel estimate of ocean oxygen utilisation points to a reduced rate of respiration in the ocean interior. *Biogeosciences*, *10*(11), 7723–7738.

Eyring, V., Bony, S., Meehl, G. A., Senior, C. A., Stevens, B., Stouffer, R. J., & Taylor, K. E. (2016). Overview of the coupled model intercomparison project phase 6 (cmip6) experimental design and organization. *Geoscientific Model Development*, *9*(5), 1937–1958.

Filella, A., Baños, I., Montero, M. F., Hernández-Hernández, N., Rodríguez-Santos, A., Ludwig, A., ... Arístegui, J. (2018). Plankton community respiration and ets activity under variable co2 and nutrient fertilization during a mesocosm study in the subtropical north atlantic. *Frontiers in Marine Science*, *5*, 310.

Fine, R. A. (2011). Observations of cfcs and sf6 as ocean tracers. *Annual review of marine science*, *3*, 173–195.

Fine, R. A., Peacock, S., Maltrud, M. E., & Bryan, F. O. (2017). A new look at ocean ventilation time scales and their uncertainties. *Journal of Geophysical Research: Oceans*, *122*(5), 3771–3798.

Ito, T., Follows, M., & Boyle, E. (2004). Is aou a good measure of respiration in the oceans? *Geophysical research letters*, *31*(17).

Ito, T., Minobe, S., Long, M. C., & Deutsch, C. (2017). Upper ocean o2 trends: 1958–2015. *Geophysical Research Letters*, *44*(9), 4214–4223.

Jenkins, W. J. (1987). 3 h and 3 he in the beta triangle: Observations of gyre ventilation and oxygen utilization rates. *Journal of Physical Oceanography*, *17*(6), 763–783.

Karstensen, J., & Tomczak, M. (1998). Age determination of mixed water masses using cfc and oxygen data. *Journal of Geophysical Research: Oceans*, *103*(C9), 18599–18609.

Koeve, W., & Kähler, P. (2016). Oxygen utilization rate (our) underestimates ocean respiration: A model study. *Global Biogeochemical Cycles*, *30*(8), 1166–1182.

Kriest, I., & Oschlies, A. (2015). Mops-1.0: towards a model for the regulation of the global oceanic nitrogen budget by marine biogeochemical processes. *Geoscientific Model Development*, *8*(9), 2929–2957.

Kwiatkowski, L., Torres, O., Bopp, L., Aumont, O., Chamberlain, M., Christian, J. R., . . . others (2020). Twenty-first century ocean warming, acidification, deoxygenation, and upper-ocean nutrient and primary production decline from cmip6 model projections. *Biogeosciences*, *17*(13), 3439–3470.

Martin, J. H., Knauer, G. A., Karl, D. M., & Broenkow, W. W. (1987). Vertex: carbon cycling in the northeast pacific. *Deep Sea Research Part A. Oceanographic Research Papers*, *34*(2), 267–285.

Matthes, K., Biastoch, A., Wahl, S., Harlaß, J., Martin, T., Brücher, T., . . . others (2020). The flexible ocean and climate infrastructure version 1 (foci1): mean state and variability. *Geoscientific Model Development*, *13*(6), 2533–2568.

Millero, F. J., & Poisson, A. (1981). International one-atmosphere equation of state of seawater. *Deep Sea Research Part A. Oceanographic Research Papers*, *28*(6), 625–629.

Oschlies, A., Brandt, P., Stramma, L., & Schmidtko, S. (2018). Drivers and mechanisms of ocean deoxygenation. *Nature Geoscience*, *11*(7), 467–473.

Pezner, A. K., Courtney, T. A., Barkley, H. C., Chou, W.-C., Chu, H.-C., Clements, S. M., . . . others (2023). Increasing hypoxia on global coral reefs under ocean warming. *Nature Climate Change*, 1–7.

Poole, R., & Tomczak, M. (1999). Optimum multiparameter analysis of the water mass structure in the atlantic ocean thermocline. *Deep Sea Research Part I: Oceanographic Research Papers*, *46*(11), 1895–1921.

Robinson, C. (2019). Microbial respiration, the engine of ocean deoxygenation. *Frontiers in Marine Science*, 533.

Schmidtko, S., Stramma, L., & Visbeck, M. (2017). Decline in global oceanic oxygen content during the past five decades. *Nature*, *542*(7641), 335–339.

Sonnerup, R. E., Chang, B. X., Warner, M. J., & Mordy, C. W. (2019). Timescales of ventilation and consumption of oxygen and fixed nitrogen in the eastern tropical south pacific oxygen deficient zone from transient tracers. *Deep Sea Research Part I: Oceanographic Research Papers*, *151*, 103080.

Sonnerup, R. E., Mecking, S., & Bullister, J. L. (2013). Transit time distributions and oxygen utilization rates in the northeast pacific ocean from chlorofluorocarbons and sulfur hexafluoride. *Deep Sea Research Part I: Oceanographic Research Papers*, *72*, 61–71.

Sonnerup, R. E., Mecking, S., Bullister, J. L., & Warner, M. J. (2015). Transit time distributions and oxygen utilization rates from chlorofluorocarbons and sulfur hexafluoride in the s outheast p acific o cean. *Journal of Geophysical Research: Oceans*, *120*(5), 3761–3776.

Sonnerup, R. E., Quay, P. D., & Bullister, J. L. (1999). Thermocline ventilation and oxygen utilization rates in the subtropical north pacific based on cfc distributions during woce. *Deep Sea Research Part I: Oceanographic Research Papers*, *46*(5), 777–805.

Stöven, T., Tanhua, T., Hoppema, M., & Bullister, J. (2015). Perspectives of transient tracer applications and limiting cases. *Ocean Science*, *11*(5), 699–718.

Stramma, L., Johnson, G. C., Sprintall, J., & Mohrholz, V. (2008). Expanding oxygen-minimum zones in the tropical oceans. *science*, *320*(5876), 655–658.

Tagliabue, A., Kwiatkowski, L., Bopp, L., Butenschön, M., Cheung, W., Lengaigne, M., & Vialard, J. (2021). Persistent uncertainties in ocean net primary produc-

441   tion climate change projections at regional scales raise challenges for assessing
442   impacts on ecosystem services. *Frontiers in Climate*, 149.
443 Thiele, G., & Sarmiento, J. (1990). Tracer dating and ocean ventilation. *Journal of*
444   *Geophysical Research: Oceans*, *95*(C6), 9377–9391.
445 Waniek, J., Koeve, W., & Prien, R. D. (2000). Trajectories of sinking particles and
446   the catchment areas above sediment traps in the northeast atlantic. *Journal of*
447   *Marine Research*, *58*(6), 983–1006.
448 Williams, P. (1981). Microbial contribution to overall marine plankton metabolism-
449   direct measurements of respiration. *Oceanologica Acta*, *4*(3), 359–364.